SINGLE AND STEREO BASED 3D METROLOGY FROM HIGH-RESOLUTION IMAGERY: METHODOLOGIES AND ACCURACIES

Arie Croitoru [a], Yong Hu [a], Vincent Tao [a], Zhizhong Xu [a], Feng Wang [b], Peter Lenson [b]

[a] GeoICT Lab, York University, 4700 Keele Street, Toronto M3J 1P3 - (arie, yhu, tao, zxu)@yorku.ca
[b] GeoTango International Corp., 4850 Keele Street, Toronto, M3J 3K1 - (fwang, plenson)@geotango.com

KEY WORDS: Three-dimensional, Metrology, Sensor, High-resolution, Imagery, Accuracy

ABSTRACT:

With the introduction of the Rational Function sensor Model (RFM) and its adoption as a primary sensor model for a verity of high-resolution sensors, the volume of imagery for which RFM data is made available is on the rise. This emerging trend is posing new opportunities for fast and reliable 2D and 3D mapping and metrology using various high-resolution sensors, while offering users a greater level of usability and interoperability. This paper examines and reviews the scheme for direct 3D information extraction from high resolution satellite imagery based on the RFM, both in single and stereo environments, and will address the issue of the attainable accuracy in each of these methods. Additionally, the methodology of 3D information extraction form high-resolution single and stereo imagery (aerial and satellite) will be presented and discussed. This paper will also examine the application of the RFM based 3D metrology scheme in a photogrammetric software environment and will provide real-world examples to the applications of 3D metrology from high-resolution imagery.

1. INTRODUCTION

Detailed 3D information is a cornerstone in a variety of applications. Nowadays, it is hard to imagine how military simulations, urban planning, navigation, emergency response, cellular communication, news and entertainment, or computer games would maintain the same level of efficiency and functionality without 3D spatial data. With the increased demand and utilization for 3D information, a need for timely and accurate metrology is also emerging. As various infrastructure systems become dependent on 3D information, timely and accurate measurement of a variety of dimensions such as heights, 3D distances, slopes or angles, becomes an essential information component. Yet, in spite this growing demand, the ability to accommodate it is still highly impaired by the availability of adequate processing methods, sensor models, calibration information, GCPs and usability. The need to explore new data sources and to provide direct 3D metrology is therefore evident.

One such data source that is becoming a dominant resource of detailed 3D metrology in various applications, are high-resolution satellite imagery (HRSI). Only a few years ago the HRSI was available to a limited number of government and defense agencies, which were utilizing such imagery using highly sophisticated software and hardware tools. The notion of widely available high-resolution satellite imagery that can be easily exploited seemed to be an unlikely reality that would not be realized in the near future. With the turn of the century this dream is rapidly becoming a reality as the world of HRSI is evolving in an unprecedented rate. Sub-meter satellite imagery is already available from a variety of commercial satellite sensors, such as the IKONOS™ and QuickBird™, in a range of formats and processing levels and at an affordable price. These types of sensors and their growing availability are revolutionizing the role of HRSI in numerous applications ranging from intelligence to insurance, media, marketing, agriculture, utilities, urban planning, forestry, environmental monitoring, transportation and real estate. The satellite data and services can be applied to almost any industry. It is estimated by some analysts that the commercial market for high-resolution satellite imagery will reach at least 30 to 40 Billion (USD) by 2005. These estimates are already being revisited with the recent emphasis on homeland security in the US and with the additional funds that are being allocated to NIMA for the purpose of purchasing high-resolution imagery.

While the satellite imagery industry has made a quantum leap in terms of resolution, data availability and quality, the available tools and paradigms to process such data into valuable user oriented information are lacking behind. Many of the available tools for processing satellite imagery are beyond the reach of most users: they still require a high level of technical expertise and are usually complex. Furthermore the challenge of providing users with robust and easy to use tools for extracting information from satellite imagery is a challenge yet to be met in many of the commercially available software tools. Although the high-resolution satellite imagery industry has progressed considerably over the last decade in terms of resolution, quality and availability, the available tools and methodologies for fast and easy processing of high-resolution imagery still pose a major barrier for most users.

One of the primary barriers to a wider adaptation and utilization of satellite imagery was the sensor model. Sensor models are a key component in restituting the functional relationships between image space and object space, and are essential in image ortho-rectification and stereo intersection. Physical sensor models are rigorous and highly suitable for adjustment by analytical triangulation and normally yield a high modeling accuracy (a fraction of one pixel). Furthermore, in physical models, parameters are statistically uncorrelated as each parameter has a physical significance. Yet, from the user's point of view, the utilization of a physical sensor model poses some difficulties. One of the primary drawbacks of the physical sensor model is that its application requires explicit understanding of each of the physical parameters and a high level of expertise. Moreover, even with complete understanding of the physical sensor model, users are still faced with the challenging task of recovering the exterior orientation of the sensor using a set of Ground Control Points

(GCPs). When no GCPs (and no inertial system telemetry) are available, users cannot recover the exterior orientation of the sensor and therefore unable to perform various mapping and data collection operations.

With the introduction of generalized sensor models, this situation has changed considerably. Generalized sensor models, particularly the RFM (Hu et al., 2004), have alleviated the requirement to obtain a physical sensor model, and with it, the requirement for a comprehensive understanding of the physical model parameters. Furthermore, as the RFM sensor model implicitly provides the interior and exterior sensor orientation, the availability of GCPs is no longer a mandatory requirement. Consequently, the use of the RFM for photogrammetric mapping is becoming a new standard in high-resolution satellite imagery that has already been implemented in various high-resolution sensors, such as Ikonos™ and QuickBird™. This has led to various research efforts that have primarily focused on the approximating accuracy (Tao and Hu, 2001), stereo intersection (Tao and Hu, 2002), correction of biases in the RFM parameters (Hu and Tao, 2002; Fraser and Hanley, 2003), block adjustment (Grodecki and Dial, 2003), and 2D/3D mapping applications (Croitoru et al., 2004).

Inspired by the advantages of the RFM and its capability to provide an open approach to photogrammetric exploitation of the commercial HRSI, the purpose of this paper is to explore how the RFM could be further utilized for extraction of 3D models. In particular, we are interested in the *user's point of view* and in demonstrating how RFM information, together with auxiliary data such as DEM, could provide an efficient, fast and economical solution that can be handled by non-expert users.

2. THE RFM FRAMEWORK

2.1 The Rational Function Model

The RFM sensor model describes the geometric relationship between the object space and image space. It relates object point coordinates (X, Y, Z) to image pixel coordinates (l, s) or vice versa using 78 rational polynomial coefficients (RPCs) that allow users to perform photogrammetric processing in the absence of the rigorous physical sensor model. For the ground-to-image transformation, the defined ratios of polynomials have the forward form (NIMA, 2000):

$$l_n = \frac{p_1(X_n, Y_n, Z_n)}{p_2(X_n, Y_n, Z_n)}, \qquad s_n = \frac{p_3(X_n, Y_n, Z_n)}{p_4(X_n, Y_n, Z_n)} \tag{1}$$

where (l_n, s_n) are the normalized row (line) and column (sample) index of pixels in image space; X_n, Y_n, and Z_n are normalized coordinate values of object points in ground space; and $p_1 \ldots p_4$ are a set of rational polynomials with coefficients a_{ijk}, b_{ijk}, c_{ijk}, d_{ijk} respectively (also called rational function coefficients (RFCs)). Each polynomial in Eq. 1 is of twenty-term cubic form. Although several versions of different permutations of the polynomial terms occur in the literature, the order defined in NIMA (2000) has been adopted by Space Imaging and Digital Globe, and thus has become the industry standard. These RFCs can be solved by terrain-independent scenario using known physical sensor models or by terrain-dependent scenario without using physical sensor models (Tao and Hu, 2001).

2.2 RFM Refinement

The RPCs provided by the vendors could be refined in image space or in object (ground) space, when additional control information becomes available. The RFM may be refined directly or indirectly (Hu et al., 2004). For example, the Ikonos *Geo* products and *Standard* stereo products will be improved to sub-meter absolute positioning accuracy using one or more high quality GCPs (Grodecki and Dial, 2003; Fraser et al, 2003; Tao and Hu, 2004) or be close to the accuracy of the GCPs whose quality is low (Hu and Tao, 2002; Tao et al. 2003). It should be noted that from the user's point of view, the availability of RFM refining methods is likely to promote the use of low cost imaging products (with a lower processing level) for various applications.

The refinement of the forward RFM can be accomplished by appending a simple complementary transformation in image space at the right-hand side of Eq. 1 in order to eliminate various error sources. The use of first-order polynomials to eliminate the image shift and drift errors as given in Eq. 2 defines an adjustable RFM model (Grodecki and Dial, 2003).

$$\begin{aligned} \Delta l &= l' - l = a_0 + a_l \cdot l + a_s \cdot s \\ \Delta s &= s' - s = b_0 + b_l \cdot l + b_s \cdot s \end{aligned} \tag{2}$$

In Eq. 2, (Δl, Δs) express the discrepancies between the measured line and sample coordinates (l', s') and the RFM projected coordinates (l, s) of a GCP or tie point; the coefficients a_0, a_l, a_s, b_0, b_l, b_s are the adjustment parameters for each image. For narrow field-of-view CCD instruments with a priori orientation data, these physical effects mainly behave like a same net effect of displacements in line and sample directions in image plane in total. Hence, for short images the error sources can be modeled by a simple translation in image space, and the above model becomes simply $\Delta l = a_0$ and $\Delta s = b_0$.

2.3 Single Image 3D Metrology

Using the refined RFCs it is possible to retrieve the 3D coordinates of points with only a single image. This is done by utilizing a dynamic measurement mode. By utilizing a DEM, it is possible to extract, for example, the 3D location of a roof point with user's cursor. Many techniques have been developed to facilitate the measurement entire process from the single image. A similar approach to the 3D point extraction could be taken by utilizing shadow information. The sun altitude and azimuth can be retrieved either from the image time or the image metadata.

This approach is particularly suitable for the extraction of building heights. However, this approach may be inapplicable in some cases due to occluded shadows, visible shadows that are projected on other objects. This approach also assumes the availability of a DEM. Although a high resolution accurate DEM will ensure the most accurate results, it is sufficient to use an approximation of the DEM or even the average relief height in some applications, such as relative building height estimation. In these cases rough estimation of the relief height may suffice due to the ratio between the building heights and the range between the building and a satellite sensor.

2.4 Stereo based 3D Metrology

When the RPCs are provided by imagery vendors or are refined using GCPs, 3-D feature extraction is possible since the RFM provides the necessary interior and exterior orientation

information (Figure 1). The reconstruction is based on the identification of two conjugate points in the stereo model. Using their image coordinates it is possible to express the relation between the left and right image coordinates and the 3D coordinates of the corresponding ground point.

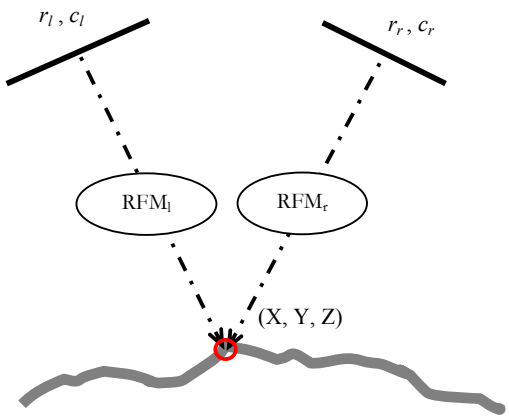

Figure 1. 3D reconstruction modes using the RFM

Let X, Y and Z to be the un-normalized coordinate values of points in object space. The normalization of the ground coordinates is computed using the following equations:

$$X_n = \frac{X - X_o}{X_s},\ Y_n = \frac{Y - Y_o}{Y_s},\ Z_n = \frac{Z - Z_o}{Z_s} \tag{3}$$

where X_o, Y_o and Z_o are offset values for three ground coordinates, and X_s, Y_s and Z_s are their scale values. The first-order approximations are obtained by applying a Taylor expansion of l and s towards the three input variables X, Y, Z in Eq. 1. Thus, when considering the normalization parameters, the four error equations for two conjugate image points (l_l, s_l) and (l_r, s_r) are derived:

$$\begin{bmatrix} v_{ll} \\ v_{sl} \\ v_{lr} \\ v_{sr} \end{bmatrix} = \begin{bmatrix} \partial l_l/\partial X/X_{sl} & \partial l_l/\partial Y/Y_{sl} & \partial l_l/\partial Z/Z_{sl} \\ \partial s_l/\partial X/X_{sl} & \partial s_l/\partial Y/Y_{sl} & \partial s_l/\partial Z/Z_{sl} \\ \partial l_r/\partial X/X_{sr} & \partial l_r/\partial Y/Y_{sr} & \partial l_r/\partial Z/Z_{sr} \\ \partial s_r/\partial X/X_{sr} & \partial s_r/\partial Y/Y_{sr} & \partial s_r/\partial Z/Z_{sr} \end{bmatrix} \cdot \begin{bmatrix} \Delta X \\ \Delta Y \\ \Delta Z \end{bmatrix} - \begin{bmatrix} l_l - \hat{l}_l \\ s_l - \hat{s}_l \\ l_r - \hat{l}_r \\ s_r - \hat{s}_r \end{bmatrix}$$

$$v = Ax - l \tag{4}$$

The reconstruction process begins with the estimation of the ground coordinates (X_0, Y_0, Z_0) obtained by solving the RFM with only constant and first-order terms, by using one image and a given elevation value, or by setting to be the offset values of the ground coordinates (Hu et al., 2004). Once retrieved, the corrections to the estimated ground coordinates are given by:

$$x = [\Delta X \ \ \Delta Y \ \ \Delta Z]^T = (A^T W A)^{-1} A^T W l \tag{5}$$

where W is the weight matrix for the image points. The weight matrix may be an identity matrix when the points are measured on images of a same sensor type. However, higher weights should be assigned to points measured in images of higher resolution when doing hybrid adjustment integrating images acquired by different sensors and thus having different resolutions (Hu et al., 2004).

2.5 SilverEye ^{TM}: An Integrated RFM Based Environment

SilverEye is a software tool that has been developed based on the RFM scheme. It has been commercialized and marketed by GeoTango International Corp. (www.geotango.com). It utilizes the RFM as the internal geometry model for various photogrammetric mapping tasks (such as ortho-rectification and stereo feature extraction). As high resolution satellite products, such as Ikonos and QuickBird are delivered with RPCs the photogrammetric process is made transparent to the users: they are no longer required to master a physical sensor model and perform interior or exterior orientation. Once an image is loaded, the corresponding RPCs are uploaded, and users are able to start performing their tasks immediately. SilverEye provides a mono (see Figure 2a) and stereo (see Figure 2b) working environments. In each of these environments users are able to collect 2D data and 3D data and organize it in a GIS-style layer format.

Figure 2a. The single image 3D mapping interface

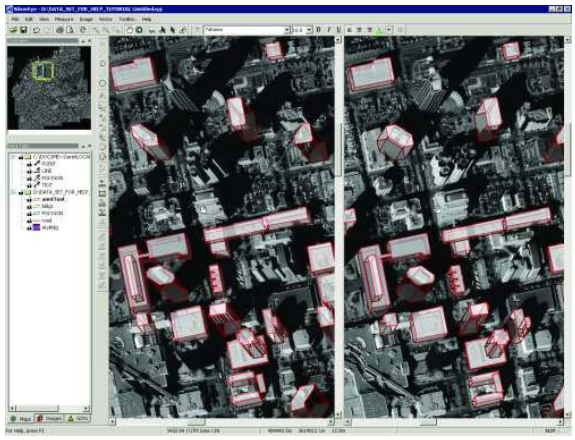

Figure 2b. The stereo image 3D mapping interface

3. EXPERIMENTAL RESULTS

Using the SilverEye package, various tests have been carried out in order to estimate its performance in two commonly used tasks: distance measurements and building height measurement.

3.1 Results With Ikonos Imagery

The test was carried out using a sample panchromatic Ikonos stereo pair (ortho-kit product level) that was provided by Space Imaging, and a 30m USGS DEM. First, the RPCs supplied with the images were refined with three high-accuracy GCPs using the refinement method described in section 2.2. The RMS errors at these GCPs before and after the refinement are given in Table 1. Then, using the above data, 33 well-distributed horizontal distances were measured using a single image and a stereo pair. In addition, measurements of the same distances were carried out in stereo using two leading commercial photogrammetric packages: PCI Geomatica© and ERDAS Imagine©. Both packages support the RFM.

	Ikonos left		Ikonos right	
	Line	Sample	Line	Sample
Original RPCs	5.37	5.34	5.21	5.04
Refined RPCs	0.57	0.12	0.57	0.32

Table 1. RMS errors in image space (Unit: pixels)

3.1.1 2D distance Measurement. An analysis of the Horizontal distance differences was carried out as the following: first the single image ("mono") measurements were compared to the stereo pair measurements that were obtained in PCI Geomatica© and ERDAS Imagine© (Figure 3a and 3b). Then the performance of the stereo processing scheme was compared to the stereo pair measurements that were obtained from the two software packages (Figure 3c and 3d). In addition, for each comparison a Gaussian curve was fitted (red curves in Figures 3a through 3e).

The summary statistics of the various comparisons are given in Table 2. The residuals that were obtained are bellow 1.5 m in all the cases as can be observed from Figure 3. No systematic effects were detected in all cases. It should also be noted that in both comparisons of mono to stereo pair measurements a higher standard deviation was obtained than in both comparisons of stereo measurements in SilverEye to stereo measurements in the other packages.

The largest standard deviation is smaller than 0.8 m for these comparisons. And this shows a sub-meter relative accuracy when measuring object dimensions using the RFM. It is interesting to note that the residuals that were obtained between SilverEye to PCI and ERDAS (Figures 3c and 3d) in the stereo measurement mode are of the same magnitude as the residuals that were obtained between PCI and ERDAS in stereo mode (Figure 3e).

	Silver Eye (mono) vs. PCI (Stereo)	Silver Eye (mono) vs. ERDAS (Stereo)	Silver Eye (stereo) vs. PCI (Stereo)	Silver Eye (stereo) vs. ERDAS (Stereo)
Mean	0.09	0.12	0.03	0.03
Std	±0.50	±0.49	±0.70	±0.72
Min	-0.85	-0.84	-1.23	-0.72
Max	1.14	1.13	0.90	0.62

Table 2. Summary statistics for mono and stereo 2D distance measurements (Unit: meters)

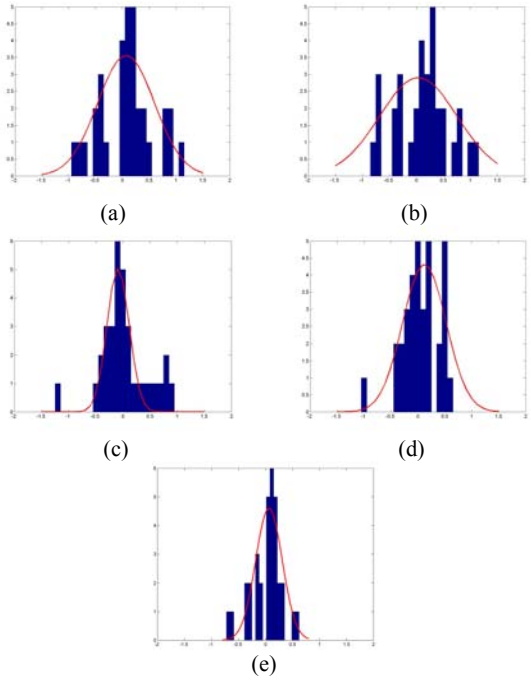

Figure 3. Evaluation of the distance difference: (a) SilverEye – mono vs. PCI – stereo; (b) SilverEye – mono vs. ERDAS Imagine – stereo; (c) SilverEye – stereo vs. PCI – stereo; (d) SilverEye – stereo vs. ERDAS Imagine – stereo (e) PCI – stereo vs. ERDAS stereo. (In all figures: x axis represents residuals in meters and y axis represents the residual frequency)

3.1.2 Height Measurement. A second test was carried out in order to evaluate the performance of the single image ("mono") and stereo-based height measurement in SilverEye. A set of 22 buildings were selected in the downtown San Diego, and four measurements were carried out for each building: mono and stereo height measurements with SilverEye, and stereo height measurements in PCI Geomatica© and ERDAS Imagine©. The results that were obtained are summarized in Table 3.

	Silver Eye (mono) vs. PCI (Stereo)	Silver Eye (mono) vs. ERDAS (Stereo)	Silver Eye (stereo) vs. PCI (Stereo)	Silver Eye (stereo) vs. ERDAS (Stereo)
Mean	0.34	0.34	-0.45	-0.45
Std	±1.54	±1.53	±0.75	±1.06
Min	-1.37	-1.74	-2.26	-2.12
Max	4.27	4.45	1.13	1.92

Table 3. Summary statistics for mono and stereo building height measurements (Unit: meters)

In this case largest residuals (above 4.0 m) were obtained for the mono measurements in comparison to the stereo measurements (bellow 2.0 m). However as can be found from Table 1, the standard deviation for single images is comparable with that for stereo images. This is because the orbit height of satellites (approximately 680 km) is significantly larger than the object heights and the shifts of terrain elevations of the building footprints in the coarse DEM relative to the true terrain

elevations have minor effects. The true terrain elevation can be obtained from stereo images with sub-meter accuracy using refined RPCs.

3.1.3. An Example Of A 3D City Model. In order to demonstrate the ability of the above-described RFM scheme to quickly and efficiently generate 3D city models, a portion of Downtown San Diego was mapped with a single IKONOS image and a DEM from the data set that was described. Each of the buildings was modeled interactively by measuring its height using the 3D floating cursor technique and digitizing the contour of its roof. Figure 4(a) depicts an example of a combined 2D and 3D data collection. Figure 4(b) depicts a photo realistic view of a draped ortho-image over the DEM and the 3D city model.

(a)

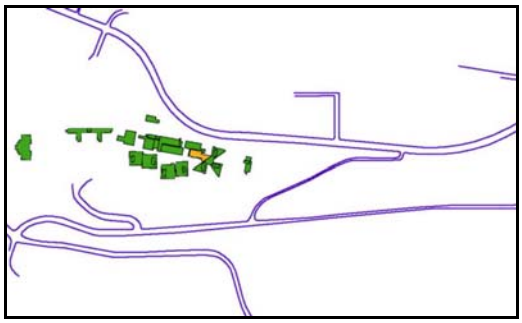

(b)

Figure 4. Mapping results with SilverEye: (a) 2D vector data collection; (b) a 3D visualization of a single image 3D mapping of downtown San Diego.

3.2 Results Using the RFM For Aerial Imagery Processing

The RFM scheme can be applied to aerial imagery using both the terrain-dependent and the terrain independent solution, To demonstrate this, an aerial stereo pair of the Ottawa city area was processed. The stereo pair covered an overlapped area of about 17 km^2. Both images had a ground resolution of 0.24 m, and were provided with the entire interior and exterior orientation parameters, the camera calibration data including fiducial marks and parameters describing the radial lens distortion. The flying height of the airplane was 2400 m above MSL. For each image, a second-order RFM was computed by the terrain-independent approach in SilverEye. The worst errors of the RFMs were 0.002 pixel in line and 0.0018 pixel in sample at the check grid points.

A topographic map sheet with the scale of 1:1250 of the study area of Ottawa city with 2-feet contours was also used. This map included the elevations of the building roofs, which are also annotated on the map (in feet). The map was compiled from aerial photography flown in May 1971 using the traditional photogrammetric processing techniques. The vertical datum and horizontal datum are Geodetic Survey of Canada (GSC) and North American Datum of 1927, respectively.

Based on this data, the heights of 12 buildings were obtained in three different ways (Table 4):

- First, the building heights are read from the map. The elevation of the base is interpolated from the map contours. However, the building base points are usually found to be higher than the surrounding terrain. Therefore these effects should be removed by subtracting the relative height of the base point relative to the terrain surface.
- Second, the building height is also measured using the projection utility on the right image. This was done by raising the cursor from the base point to the building roof along the side of the buildings. Because we do not have a DTM, the average terrain elevation (82.6 m MSL) is used to approximate the elevations of the building footprints. If the average elevation is increase to 120 m MSL, then the measured heights will be 0.51 m smaller in average than those listed in Table 4. While the mean error is 0.34 m for Ikonos as shown in Table 3. So this effect is more significant for aerial images than satellite images.
- Third, the elevations of the building base, the terrain and the roof were measured using stereo pair. The terrain elevation is intended to eliminate the effect of higher base over terrain when compared with the figures read from the map. Consequently, we measured the height correction (the last column in Table 4) of the base point relative to the natural terrain using the stereo pair to eliminate this systematic bias of heights since such data cannot be read from the map. These height corrections are all positive values, and this show that the building footprints are usually higher than their surroundings.

The differences between the building heights obtained using the above three ways are compared in Tables 5 and 6, respectively with and without systematic biases. It can be observed that the largest difference is 0.9 m only when comparing the stereo-based heights and the corrected map heights. Overall, as can be observed from Table 6, the heights measured using stereo images were more accurate than those using a single image.

4. CONCLUSIONS

The RFM framework provides a comprehensive photogrammetric solution in a variety of applications. It offers greater flexibility and enables non-technical users to exploit the full potential of high-resolution imagery. Using this framework, users are able to overcome two traditional barriers in photogrammetric processing, namely the requirement for a physical sensor model and the requirement of triangulation using GCPs for deriving the sensor orientation.

In contrast to this, it should be noted that currently the implementation of the RFM scheme and its adaptation in practice heavily depends on data vendors. As users are not provided with tools to generate their own RPCs, their ability to adopt and utilize the RFM framework depends on the availability of RPCs that are supplied with the raw imagery data. Yet, as this new framework is being rapidly adopted for

new and existing sensors, and a growing number of "RFM enabled" commercial tools are made available.

This paper discussed the single image based 3-D feature extraction and compared these results with those measured using stereo images. It has also demonstrated the application of single image processing for 3D city model generation. It should be noted that single image 3D reconstruction methods are of great importance in the case of the HRSI due to the somewhat limited availability of stereo pairs.

Although single image height measurement and 3D reconstruction offer greater flexibly and lower costs, human measurement errors, such as misidentification of the base or roof of a building in one image, can affect the accuracy of height measurement. It is therefore important to carefully design and provide utilities to assist users on performing 3D extraction from the single imagery.

The paper also discussed the extension of the RFM to aerial imagery. This included the generation of the RFM coefficients based on the known exterior orientation using the terrain independent scheme. Overall, these preliminary results suggest that sub-meter accuracies can be achieved.

	Map in GSC				*Single (m)*	*Stereo (m)*			
No.	Terrain elevation (feet)	Roof elevation (feet)	Height relative to terrain (m)	Height relative to base (m)	Height	Base elevation (MSL)	Height	Terrain elevation	Height correction
1	236	357	36.9	36.3	37.8	73.7	36.2	73.1	0.6
2	235	397	49.4	47.5	49.2	73.7	48.3	71.8	1.9
3	236	521	86.9	86.2	87.3	73.3	86.0	72.6	0.7
4	236	521	86.9	86.2	87.2	73.3	86.1	72.6	0.7
5	232	554	98.2	92.1	91.9	77.0	91.2	70.9	6.1
6	232	327	29.0	22.9	23.7	77.0	22.8	70.9	6.1
7	232	335	31.4	25.3	26.1	77.0	25.2	70.9	6.1
8	232	350	36.0	29.9	31.0	77.0	30.0	70.9	6.1
9	240	353	34.5	33.2	33.5	75.4	33.1	74.1	1.3
10	240	378	42.1	40.8	41.9	75.4	41.0	74.1	1.3
11	235	453	66.5	65.0	63.7	73.1	65.5	71.6	1.5
12	235	470	71.6	70.1	68.9	73.1	70.2	71.6	1.5

Table 4. Building Heights obtained in three ways

	Stereo vs. Map	Single vs. Map	Single vs. Stereo
Mean	-2.82	-2.27	0.55
Std	2.63	2.64	1.03
RMS	3.78	3.39	1.13
Max Abs.	7.00	6.30	1.80

Table 5. Differences with systematic vertical shifts (m)

	Stereo vs. Corrected map	Single vs. Corrected map	Map vs. Corrected map
Mean	-0.01	0.56	2.83
Std	0.41	0.98	2.45
RMS	0.39	1.09	3.67
Max Abs.	0.90	1.70	6.10

Table 6. Differences without systematic vertical shifts (m)

5. REFERENCES

Croitoru, A. Tao, V., Hu, Y., Xu, J. Wang, F. and Lenson, P., 2004. The rational function model: a unified 2D and 3D spatial data generation scheme. *ASPRS annual Conference*, 23-28 May, Denver, Colorado, 11 pages

Fraser, C., Hanley, H., 2003. Bias compensation in rational functions for Ikonos satellite imagery. *PE&RS*, 69, pp. 53-57.

Grodecki, J., Dial, G., 2003. Block adjustment of high resolution satellite images described by rational polynomials. *PE&RS*, 69(1), pp. 59-68.

Hu, Y., Tao, V., 2002. Updating solutions of the rational function model using additional control information. *PE&RS*, 68(7), pp. 715-724.

Hu, Y., Tao, V., Croitoru, A., 2004. Understanding the rational function model: methods and applications. *IAPRS*, 12-23 July, Istanbul, vol. XX, 6 p.

NIMA, 2000. *The Compendium of Controlled Extensions (CE) for the National Imagery Transmission Format* (Version 2.1). (http://164.214.2.51/ntb/baseline/stdi00021/stdi00021.pdf)

Tao, V., Hu, Y., 2001. A comprehensive study on the rational function model for photogrammetric processing. *PE&RS*, 67(12), pp. 1347-1357.

Tao, V., Hu, Y., 2002. 3-D reconstruction algorithms with the rational function model. *PE&RS*, 68(7), pp. 705-714.

Tao, V., Hu, Y., 2004. RFM: an open sensor model for cross sensor mapping. *ASPRS annual Conference*, 23-28 May, Denver, Colorado, 9 pages.